

An Efficient Robust Algorithm for the Surface-Potential Calculation of Independent DG MOSFET

Srivatsava Jandhyala and Santanu Mahapatra, *Senior Member, IEEE*

Abstract—Although the recently proposed single-implicit-equation-based input voltage equations (IVEs) for the independent double-gate (IDG) MOSFET promise faster computation time than the earlier proposed coupled-equations-based IVEs, it is not clear how those equations could be solved inside a circuit simulator as the conventional Newton–Raphson (NR)-based root finding method will not always converge due to the presence of discontinuity at the G-zero point (GZP) and nonremovable singularities in the trigonometric IVE. In this paper, we propose a unique algorithm to solve those IVEs, which combines the Ridders algorithm with the NR-based technique in order to provide assured convergence for any bias conditions. Studying the IDG MOSFET operation carefully, we apply an optimized initial guess to the NR component and a minimized solution space to the Ridders component in order to achieve rapid convergence, which is very important for circuit simulation. To reduce the computation budget further, we propose a new closed-form solution of the IVEs in the near vicinity of the GZP. The proposed algorithm is tested with different device parameters in the extended range of bias conditions and successfully implemented in a commercial circuit simulator through its Verilog-A interface.

Index Terms—Circuit simulation, compact modeling, double-gate MOSFET, input voltage equations (IVEs).

I. INTRODUCTION

THE independent double-gate (IDG) MOSFET has received considerable attention in the recent years, owing to its ability to modulate the threshold voltage and the transconductance dynamically. A fast and accurate solution of the input voltage equations (IVEs) is the most fundamental step toward developing surface-potential-based compact models for such transistors. Previous techniques [1]–[4] used for solving the 1-D Poisson equation (PE) rigorously for long-channel IDG MOSFETs result in IVEs that involve multiple intercoupled implicit equations, which are computationally expensive for circuit simulation. Recently, we have proposed a different

rigorous technique for solving the same PE by which one can obtain single-implicit-equation-based IVEs [5] (there are four independent implicit equations; however, for a given bias condition, we need to solve only one of them). By using the optimization routine available in a commercial computational software program [6], we show that the single-implicit-equation-based IVEs converge five times faster than the coupled-implicit-equation-based IVEs. However, it is difficult to make such optimization routines converge, and they are also not available in standard “C” or “Verilog-A” libraries.

Finding the solution of the IVEs for the IDG MOSFET is quite a nontrivial exercise due to the following reasons. In comparison to the bulk and symmetric double-gate (SDG) MOSFETs, the complexities in the IVEs of the IDG MOSFET are manifolds. Here, the IVEs can take two different forms, i.e., trigonometric (when the external-bias-dependent coupling factor $G \leq 0$ [5]) or hyperbolic ($G > 0$), and thus, the IVEs are discontinuous at $G = 0$ [(G-zero point (GZP))]. In addition, the trigonometric IVE has several nonremovable singularities due to the presence of $\cot(\cdot)$ and $\log[\sin(\cdot)]$ terms. As a result, the Newton–Raphson (NR)-based method either does not converge (leads to an imaginary solution) or very slowly converge when the root of the IVEs lies close to the discontinuity/singularity points. Moreover, the higher order derivatives of the IVEs are extremely cumbersome, and thus, it is impractical to constitute a higher order NR method for faster convergence. In order to achieve assured convergence, one needs to use a computationally expensive bisection method. Furthermore, it can be seen that the analytical approximations proposed for bulk [7] and SDG MOSFETs [8] are not applicable to the IVEs of the IDG MOSFET.

In this paper, we propose a unique algorithm to solve the IVEs [5], which combines the Ridders algorithm [9] with the NR-based technique in order to provide assured convergence with a low computational budget for any bias conditions. The Ridders algorithm is a *bounded* root finding technique, which offers assured convergence at a much faster rate than the regular bisection routine. Studying the IDG MOSFET operation carefully, we apply an optimized initial guess to the NR component and a minimized solution space to the Ridders component in order to achieve rapid convergence, which is very important for circuit simulation. To reduce the computation budget further, using the concept of the GZP, we propose a new closed-form solution of the IVEs in the very near vicinity of the GZP. The proposed algorithm is implemented in a Verilog-A-based

Manuscript received December 2, 2010; accepted March 14, 2011. This work was supported by the Department of Science and Technology, India, under Grant SR/S3/EECE/047/2008. The review of this paper was arranged by Editor D. Esseni.

The authors are with the Nano Scale Device Research Laboratory, Center for Electronics Design and Technology, Indian Institute of Science, Bangalore 560012, India (e-mail: srivatsava@cedt.iisc.ernet.in; santanu@cedt.iisc.ernet.in).

Color versions of one or more of the figures in this paper are available online at <http://ieeexplore.ieee.org>.

Digital Object Identifier 10.1109/TED.2011.2131654

circuit simulator [10], tested and verified against numerical simulations [11], [12].

It is worth noting that coupled-implicit-equation-based IVEs also have similar discontinuity and singularity points. However, as it is extremely difficult to constitute an efficient *bounded* root finding technique for the *multidimensional solution space* [13], those IVEs appear to be more theoretical in nature than useful for the practical implementation in a circuit simulator. A similar argument is also applicable for a recent work [14] that uses complex variable and multiple coupled equations.

II. DEVELOPMENT OF THE ALGORITHM

Conventions used in this paper are follows: $C_{\text{ox}1(2)}$ is the oxide capacitance per unit area of the first (second) gate defined as $\epsilon_{\text{ox}}/t_{\text{ox}1(2)}$, C_{si} is the silicon body capacitance per unit area defined as $\epsilon_{\text{si}}/t_{\text{si}}$, ϵ_{si} and ϵ_{ox} are the permittivities, and t_{si} and t_{ox} are the thicknesses of silicon and SiO₂, respectively. q is the elementary charge, β is the inverse thermal voltage, n_i is the intrinsic carrier density, V is the electron quasi-Fermi potential (channel potential), $\psi_{1(2)}$ Si/SiO₂ is the interface potential at first (second) gate, and $V_{g_{s1(2)}}$ is the effective front (back)-gate voltage, i.e., $V_{g_{s1(2)}} = V_{g_{s1(2)\text{applied}}} - \Delta\phi_{1(2)}$, where $\Delta\phi_{1(2)}$ is the work function difference at the respective gates.

We explain the algorithm for case $V_{g_{s1}} \geq V_{g_{s2}}$, and it could be extended in similar lines for case $V_{g_{s1}} < V_{g_{s2}}$. The hyperbolic ($f_{\text{hyp}1}(\psi_1) = 0$) and trigonometric ($f_{\text{trig}1}(\psi_1) = 0$) equations for which we are seeking the solutions are given below:

$$f_{\text{hyp}1} \equiv -\sqrt{\frac{Be^{-\beta V}}{G_1}} \sinh\theta_1 + e^{-\frac{\beta \left(V_{g_{s2}} + \frac{\sqrt{G_1} \epsilon_{\text{si}} \coth\theta_1}{C_{\text{ox}2}} \right)}{2}} \quad (1)$$

$$f_{\text{trig}1} \equiv \frac{e^{\frac{\sqrt{G_1} \beta \epsilon_{\text{si}} \cot\theta_1^*}{2C_{\text{ox}2}}} \sin\theta_1^*}{\sqrt{G_1^*}} - \sqrt{\frac{e^{-\beta(V_{g_{s2}}-V)}}{B}} \quad (2)$$

where

$$G_1 = \frac{C_{\text{ox}1}^2 (V_{g_{s1}} - \psi_1)^2}{\epsilon_{\text{si}}^2} - Be^{\beta(\psi_1 - V)} \quad (3)$$

$$\theta_1 = \frac{\sqrt{G_1} \beta t_{\text{si}}}{2} + \sinh^{-1} \left(\frac{\sqrt{G_1}}{\sqrt{Be^{\beta(\psi_1 - V)}}} \right) \quad (4)$$

with $B = (2qn_i)/(\beta\epsilon_{\text{si}})$ and $G_1^* = -G_1$. θ_1^* could be obtained by replacing G_1 with G_1^* and \sinh^{-1} with \sin^{-1} in (4). These equations are obtained by restructuring the IVEs proposed in [5] for better convergence.

A. $\psi_{\text{gzp}1}$ Calculation

As explained in [5], the surface-potential computation should start with the $\psi_{\text{gzp}1}$ calculation, which is the solution of the $2G_1 = 0$ equation. As the IVEs are discontinuous at the GZP, $\psi_{\text{gzp}1}$ needs to be calculated with very high accuracy. Although a closed-form solution of $\psi_{\text{gzp}1}$ is available in terms of the Lambert W function and can be implemented in a simulator as discussed in [15], such an expression has following limitations: 1) The exponential term inside the argument of the W function overflows for high values of $(V_{g_{s1}} - V)$ (for example, beyond

36 V at room temperature for a long double-precision data-type implementation) and thus becomes uncomputable for large bias values, which might appear during circuit simulation [16]. 2) The implementation of the W function in special C libraries or in mathematical packages are generic in nature. For example, in the GNU Scientific Library (GSL) [17], the W function is computed using Halley's method with some optimized initial guess (obtained from the polynomial approximation of the W function). It is possible to reduce the computation time of $\psi_{\text{gzp}1}$ if we try to solve equation $G_1 = 0$ directly using a physics-based initial guess. In this paper, we calculate $\psi_{\text{gzp}1}$ by transforming equation $G_1 = 0$ into the following form:

$$f_{\psi_{\text{gzp}1}} \equiv V_{g_{s1}} - \psi_1 - \frac{\epsilon_{\text{si}} \sqrt{Be^{\beta(\psi_1 - V)}}}{C_{\text{ox}1}} = 0. \quad (5)$$

We then solve this equation by Halley's method using the initial guess $V_{g_{s1}}$ for $V_{g_{s1}} \leq 0$ and $\min((2/\beta) \ln(V_{g_{s1}} C_{\text{ox}1} / \epsilon_{\text{si}} \sqrt{B}) + V, V_{g_{s1}})$ for other values with the exit condition $|f_{\psi_{\text{gzp}1}}| < 10^{-17}$ or when the absolute difference between $\psi_{\text{gzp}1}$ obtained from two successive iterations becomes less than 10δ (where δ is the machine precision and, for a long double data type, δ is equal to $2^{-52} \approx 2.3 * 10^{-16}$). In most of the cases, the Halley loop is seen to converge within two to three iterations. We present the comparison of the performance of our proposed implementation to that of the Lambert-function-based approach in Section III.

We then use $\psi_{\text{gzp}1}$ to calculate the value of the critical gate voltage $V_{g_{s2}\text{crit}}$ (as it appears in [5]) in order to choose between trigonometric or hyperbolic IVE.

B. Explicit Solution

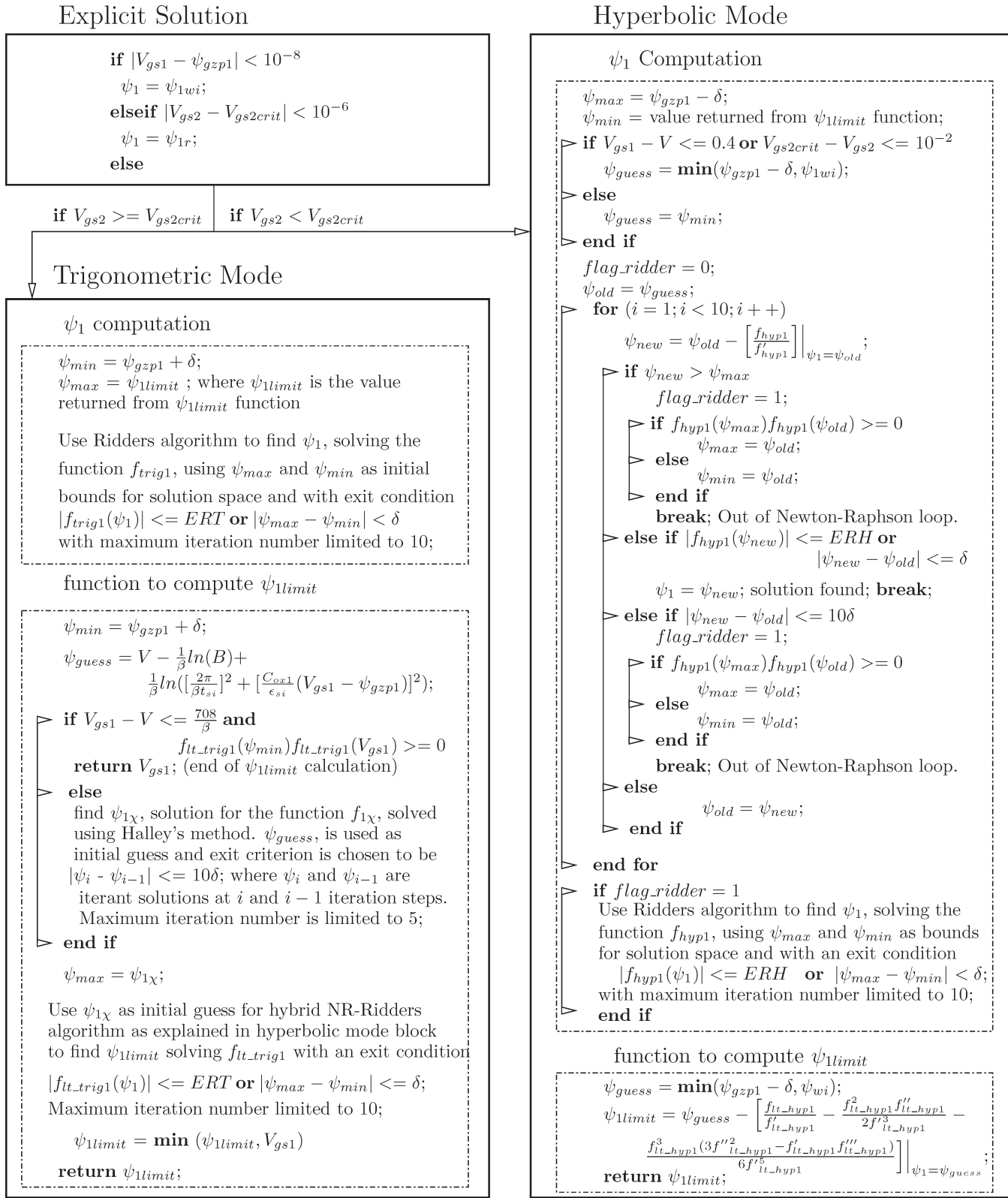
For a given bias point, ψ_1 is determined, as depicted by the algorithm in Fig. 1. Here, we first check for the cases where ψ_1 can be approximated to an explicit form in order to reduce the computation budget. As explained in [5], at deep weak inversion, the difference between $\psi_{\text{gzp}1}$ and $V_{g_{s1}}$ becomes extremely small, and then, the surface potential could be approximated by the following expression of $\psi_{1\text{wi}}$ by neglecting the inversion charge completely:

$$\psi_{1\text{wi}} = \frac{V_{g_{s1}}}{1 + \frac{C_{\text{ox}2} C_{\text{si}}}{C_{\text{ox}1} C_{\text{si}} + C_{\text{ox}1} C_{\text{ox}2}}} + \frac{V_{g_{s2}}}{\frac{C_{\text{ox}1} C_{\text{si}} + C_{\text{ox}1} C_{\text{ox}2}}{C_{\text{ox}2} C_{\text{si}}} + 1}. \quad (6)$$

Another explicit formulation of the surface potential is possible when $V_{g_{s2}}$ is very close to $V_{g_{s2}\text{crit}}$ (i.e., the solution is very close to the $\psi_{\text{gzp}1}$ value). Here, using the concept of the GZP, a generic explicit formulation for the surface potential could be obtained by Taylor series expansion with respect to $V_{g_{s2}}$ around the GZP as given below:

$$\psi_1 = \psi_{\text{gzp}1} + \sum_n \frac{1}{n!} \left. \frac{\partial^n \psi_1}{\partial V_{g_{s2}}^n} \right|_{\psi_1 = \psi_{\text{gzp}1}} (V_{g_{s2}} - V_{g_{s2}\text{crit}})^n. \quad (7)$$

Unfortunately such expression cannot be used in the circuit simulator as it is very difficult to obtain the analytical


 Fig. 1. Algorithm for finding roots of the IDG-MOSFET IVEs. ERT , ERH are adjustable parameters chosen to be 10^{-17} and 10^{-13} respectively in this work.

expressions for higher order derivatives $\partial^n \psi_1 / \partial V_{gs2}^n$ at the GZP. However, if we neglect all the higher order terms in (7), then in the close neighborhood of the GZP, ψ_1 could be approximated as $\psi_1 \simeq \psi_{1r} = \psi_{gzp1} + (\partial \psi_1 / \partial V_{gs2})|_{\psi_1 = \psi_{gzp1}} (V_{gs2} -$

$V_{gs2crit})$, where the expression for $\partial \psi_1 / \partial V_{gs2}|_{\psi_1 = \psi_{gzp1}}$ is obtained from the IVEs (either from the trigonometric or hyperbolic one) and given in (8), shown at the bottom of the next page.

The bias ranges for which such solutions could be used in the algorithm is heuristically chosen such that the continuity in the surface potential, the drain current, and the transconductances is well preserved. If conditions for using those explicit solutions are not satisfied, the IVEs are numerically solved. The explicit solution also helps us avoid the computation of IVEs (1) and (2) around the GZP, which is numerically unstable, since $\cot(\theta)$ and $\coth(\theta) \rightarrow \infty$ as $G \rightarrow 0$.

C. Solution of the Hyperbolic IVE

In order to solve $f_{\text{hyp}1}$, we first use the NR algorithm with the optimized initial guess and then switch to the Ridders algorithm if NR fails to converge. In order to use the Ridders algorithm, we first need to calculate the solution space (i.e., maximum and minimum possible values of ψ_1). In the hyperbolic mode, $\psi_1 < \psi_{\text{gzp}1}$ [5], and thus, the maximum bound for $f_{\text{hyp}1} = 0$ is $\psi_{\text{gzp}1}$. The lower bound could be obtained in following manner. When G_1 becomes large, [5, eq. (11)] could be approximated as

$$\frac{C_{\text{ox}2}}{\epsilon_{\text{si}}} \left[\frac{2}{\beta} \left\{ \ln \left(\sqrt{\frac{B e^{-\beta V}}{G_1}} \right) + \theta_1 - \ln 2 \right\} + V_{\text{gs}2} \right] + \sqrt{G_1} = 0. \quad (9)$$

The solution of (9) gives the lower bound of ψ_1 in $f_{\text{hyp}1}$. However, this equation is difficult to solve. Since $\sinh^{-1}(x) > \ln(2x)$ for all positive and finite x values and $\ln(2x)$ is a curvilinear asymptote of $\sinh^{-1}(x)$, by replacing term $\sinh^{-1}(\sqrt{G_1}/\sqrt{B e^{\beta(\psi_1 - V)}}) - \ln 2$ with $\ln(\sqrt{G_1}/\sqrt{B e^{\beta(\psi_1 - V)}})$ in the expression for θ_1 in (9), we arrive at the following simpler function $f_{\text{lt_hyp}1}$, the solution of which, i.e., $\psi_{1\text{limit}}$, provides the lower bound of ψ_1 :

$$f_{\text{lt_hyp}1} \equiv B e^{-\beta(V - \psi_1)} - \frac{C_{\text{ox}1}^2}{\epsilon_{\text{si}}^2} (V_{\text{gs}1} - \psi_1)^2 + \frac{C_{\text{ox}2}^2}{\epsilon_{\text{si}}^2 \left(\frac{C_{\text{ox}2}}{C_{\text{si}}} + 1 \right)^2} (V_{\text{gs}2} - \psi_1)^2. \quad (10)$$

Using the technique discussed in [8], an approximate analytical solution of (10) is obtained, as shown in Fig. 1.

To solve $f_{\text{hyp}1}$ when $V_{\text{gs}1} - V \leq 0.4$ or $V_{\text{gs}2\text{crit}} - V_{\text{gs}2} \leq 0.01$, the initial guess ψ_{guess} for NR is chosen to be $\min(\psi_{\text{gzp}1} - \delta, \psi_{1\text{wi}})$ since the device will be either in weak inversion or close to the GZP. For other biases, ψ_{guess} is taken to be $\psi_{1\text{limit}}$. The derivative of $f_{\text{hyp}1}$ is given in (11). As one can see, the expression of $f'_{\text{hyp}1}$ is pretty complicated, and thus, it is impractical to constitute the higher order NR method using higher order derivatives. The NR loop successfully converges if $|f_{\text{hyp}1}| < 10^{-13}$ or the change in ψ_1 between two successive iterations, i.e., $|\psi_{\text{new}} - \psi_{\text{old}}|$, is less than δ .

As mentioned earlier, $f_{\text{hyp}1}$ is discontinuous at the GZP, and thus, for many practical biases, the NR loop might not converge if, at any stage, the iterative solution becomes higher than $\psi_{\text{gzp}1}$. For such cases, we have to switch to the Ridders algorithm. We implement the Ridders algorithm as it appears in [18] with ψ_{max} and ψ_{min} representing quantities x_h and x_l , respectively. A slight modification is made to eliminate the cases where the proposed implementation might fail. When the S-parameter given in [18] goes to zero or $(1 - |(\mathcal{F}(\psi_{\text{max}} + \psi_{\text{min}}/2))/S| < 10\delta)$, where \mathcal{F} is the function to be solved by the Ridders algorithm, then the bisection algorithm is used as backup to assure certain convergence. This situation is however very less probable, as shown in the results presented Section III. As shown in Fig. 1, a flag *flag_ridder* gets set whenever ψ_{new} exceeds $\psi_{\text{gzp}1}$. It also gets set when the relative change in the solution between iterations $|\psi_{\text{new}} - \psi_{\text{old}}|$ is less than 10δ , which is an empirical check for slow NR convergence or oscillations in convergence. When this flag gets set, the Ridders algorithm gets executed after breaking out of the NR loop. For the Ridders method, the ideal bounds for the solution spaces are $\psi_{\text{gzp}1}$ and $\psi_{1\text{limit}}$. However, in the hyperbolic mode, $\psi_{1\text{limit}}$ can be very far from $\psi_{\text{gzp}1}$, and thus, the Ridders algorithm might slowly converge. The interim solution ψ_{old} obtained in the NR loop is used to reduce the bounds of the solution space. As shown in Fig. 1, the sign of function $f_{\text{lt_hyp}1}$ at the interim solution $\psi = \psi_{\text{old}}$ is compared with its sign at $\psi = \psi_{\text{gzp}1}$. If the sign is negative, then the lower bound can be changed from $\psi_{1\text{limit}}$ to ψ_{old} , else the upper bound can be changed from

$$\left. \frac{\partial \psi_1}{\partial V_{\text{gs}2}} \right|_{\psi_1 = \psi_{\text{gzp}1}} = (12\alpha_1^2 C_{\text{ox}2} \epsilon_{\text{si}}^2 (\alpha_1 \beta t_{\text{si}} + 2)^3) \left/ \left(\frac{B^3 \beta^4 \epsilon_{\text{si}}^2 t_{\text{si}}^3 (16\epsilon_{\text{si}} + 10C_{\text{ox}2} t_{\text{si}} + \alpha_1 \beta C_{\text{ox}2} t_{\text{si}}^2 + 2\alpha_1 \beta \epsilon_{\text{si}} t_{\text{si}})}{e^{3\beta(V - \psi_{\text{gzp}1})}} + \frac{16BC_{\text{ox}2} (\epsilon_{\text{si}}^2 (9\alpha_1 \beta t_{\text{si}} + 6) - \beta t_{\text{si}}^2 \omega_1 (5\alpha_1 \beta t_{\text{si}} + 9)) B (48\beta \epsilon_{\text{si}} t_{\text{si}} \omega_1 (2\alpha_1 \beta t_{\text{si}} + 3))}{e^{\beta(V - \psi_{\text{gzp}1})}} - 96\alpha_1 \omega_1 (\epsilon_{\text{si}} + C_{\text{ox}2} t_{\text{si}}) + \frac{2B^2 \beta^2 t_{\text{si}} (\epsilon_{\text{si}}^3 (24\alpha_1 \beta t_{\text{si}} + 24) + 4C_{\text{ox}2} \epsilon_{\text{si}}^2 t_{\text{si}} (5\alpha_1 \beta t_{\text{si}} + 12))}{e^{2\beta(V - \psi_{\text{gzp}1})}} + \frac{2B^2 \beta^2 t_{\text{si}} (-\beta C_{\text{ox}2} t_{\text{si}}^3 \omega_1 (\alpha_1 \beta t_{\text{si}} + 10)) - (2\beta \epsilon_{\text{si}} t_{\text{si}}^2 \omega_1 (\alpha_1 \beta t_{\text{si}} + 8))}{e^{2\beta(V - \psi_{\text{gzp}1})}} \right)$$

where $\alpha_1 = \sqrt{B e^{-\beta(V - \psi_{\text{gzp}1})}}$ and $\omega_1 = C_{\text{ox}1}^2 (\psi_{\text{gzp}1} - V_{\text{gs}1})$ (8)

ψ_{gzp1} to ψ_{old} . The search space, hence, is now limited to either ψ_{old} to ψ_{1limit} or ψ_{old} to ψ_{gzp1} instead of ψ_{1limit} to ψ_{gzp1} . In this way, even in cases where NR does not converge, we can use its interim solution ψ_{old} to reduce the search space, which remarkably improves the efficiency of the Ridders algorithm

$$f'_{hyp1} = -\sqrt{\frac{Be^{-\beta V}}{G_1}} \cosh(\theta_1)\kappa_1 + \frac{\sqrt{Be^{-\beta V}} \sinh(\theta_1)\gamma_1}{2G_1^{\frac{3}{2}}} - \frac{\beta \left(\frac{\epsilon_{si} \coth(\theta_1)\gamma_1}{2C_{ox2}\sqrt{G_1}} - \frac{\epsilon_{si}\sqrt{G_1}(\coth^2(\theta_1)-1)\kappa_1}{C_{ox2}} \right)}{2 \frac{\beta \left(V_{gs2} + \frac{\epsilon_{si}\sqrt{G_1} \coth(\theta_1)}{C_{ox2}} \right)}{e}}.$$

where

$$\begin{aligned} \gamma_1 &= \frac{\partial G_1}{\partial \psi_1} \\ &= \frac{2C_{ox1}^2(\psi_1 - V_{gs1})}{\epsilon_{si}^2} - \beta B e^{-\beta(V-\psi_1)} \\ \kappa_1 &= \frac{\partial \theta_1}{\partial \psi_1} \\ &= -\frac{\beta t_{si}\gamma_1}{4\sqrt{G_1}} - \frac{2e^{\frac{\beta\psi_1}{2}} \sqrt{\frac{B}{G_1 e^{\beta V}}} + \frac{B\gamma_1}{2G_1^2 e^{\beta V} e^{\frac{\beta\psi_1}{2}} \left(\frac{B}{G_1 e^{\beta V}}\right)^{\frac{3}{2}}}}{\sqrt{\frac{G_1 e^{\beta(V-\psi_1)}}{B}} + 1}. \end{aligned} \quad (11)$$

D. Solution of the Trigonometric IVE

To solve $f_{trig1} = 0$, we use only the Ridders algorithm as the solution space is much smaller (five to ten times) than the hyperbolic case, where the Ridders method is found to show similar or even better performance than the NR or hybrid NR–Ridders method. Moreover, the Ridders algorithm does not require the derivative of the function to be solved. As the derivatives of the IVEs are pretty complicated, the implementation of the Ridders algorithm is less error prone than the NR routine. The lower bound for the solution space is ψ_{gzp1} as in the trigonometric mode $\psi_1 > \psi_{gzp1}$ [5]. From the expression of f_{trig1} , one can deduce that the upper bound of the solution space ψ_{1limit} is determined by the solution of equation $f_{1t_trig1} \equiv \pi - \theta_1^* = 0$, which also denotes the first nonremovable singularity point of f_{trig1} and thus needs to be very accurately evaluated. Unlike f_{hyp1} , the solution space of f_{trig1} is bounded between a discontinuity point and a singularity point, which gives another argument to use pure Ridders method for root finding.

A straightforward NR-based method is found to be not efficient for solving f_{1t_trig1} , as during iteration, $\sqrt{G_1^*}$ could become imaginary, and thus, we use the hybrid NR–Ridders method (similar to the hyperbolic mode). To solve f_{1t_trig1} by the Ridders method, we need to find the upper bound of ψ_{1limit} (the lower bound is given by ψ_{gzp1}). Now, as the maximum possible value of $\sqrt{G_1^*}$ could be $2\pi/(\beta t_{si})$ [1], the solution of equation $\pi - (\beta\sqrt{G_1^*}t_{si}/2) = 0$, denoted by $\psi_{1\chi}$, provides the upper bound of ψ_{1limit} . This equation for computing $\psi_{1\chi}$ can

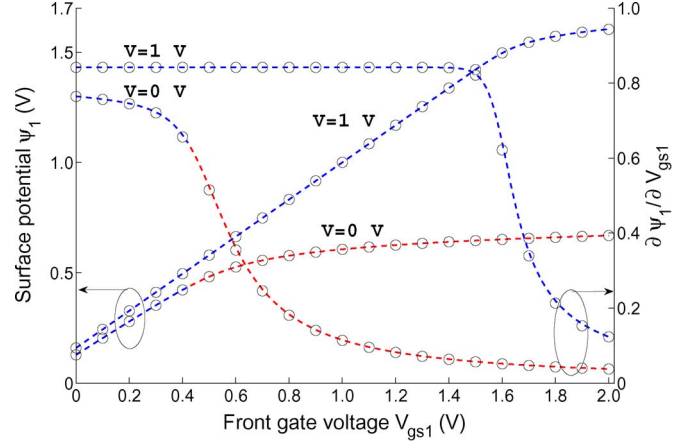


Fig. 2. Comparison of (dotted line) the proposed algorithm with (circle) the COMSOL solution. (Blue) Hyperbolic mode. (Red) Trigonometric mode. The device parameters are $t_{ox1} = 1$ nm, $t_{ox2} = 2$ nm, $t_{si} = 10$ nm, and $V_{gs2} = 1$ V.

be transformed into following form, which can eliminate the discontinuities at boundaries and has better convergence:

$$f_{1\chi} \equiv V - \psi + \frac{\ln\left(\frac{4\pi^2}{\beta^2 t_{si}^2} + \frac{C_{ox1}^2(\psi - V_{gs1})^2}{\epsilon_{si}^2}\right)}{\beta} - \frac{\ln(B)}{\beta}. \quad (12)$$

$f_{1\chi}$ can be solved using Halley's method, as shown in Fig. 1. Although the solution of f_{1t_trig1} gives the *ideal* upper bound for the surface potential, it can be further reduced to optimize the solution space of f_{trig1} . In order to do so, we use the fact that $\psi_1 \leq V_{gs1}$; however, ψ_{1limit} could be greater than V_{gs1} . As shown in Fig. 1, if V_{gs1} is less than ψ_{1limit} , then the upper bound for ψ_1 is simply V_{gs1} , and thus, the computation of ψ_{1limit} can be avoided. This check is done even before the computation of $\psi_{1\chi}$ by comparing the sign of function f_{1t_trig1} at $\psi = V_{gs1}$ with that of $\psi = \psi_{gzp1}$. This optimization in the upper bound of ψ_1 is found to provide significant improvement in the overall computation time, as we not only avoid the overhead (ψ_{1limit}) computation, but we also reduce the solution space for the solution in $f_{trig1} = 0$. It will be shown in Section III that the overhead computation time is quite small compared with the total computational-time Ridders loop in (2), and thus, the reduction in its solution space will improve the overall performance significantly. However, this check has a numerical limitation. It can be performed only when $V_{gs1} - V < 708/\beta$, as beyond this point, the exponential term in the expression of f_{1t_trig1} overflows (similar to the ψ_{gzp1} calculation). Hence, for cases $V_{gs1} - V > 708/\beta$, the aforementioned bound optimization is performed after the computation of ψ_{1limit} . Once the optimized upper bound for ψ_1 is obtained, f_{trig1} is solved using the Ridders method, as explained in Fig. 1.

III. RESULTS AND DISCUSSION

We validate the accuracy of our algorithm against the numerical solution of the PE obtained from the COMSOL 4.0 multiphysics software [12]. Fig. 2 shows the good agreement between results obtained from the proposed algorithm and the

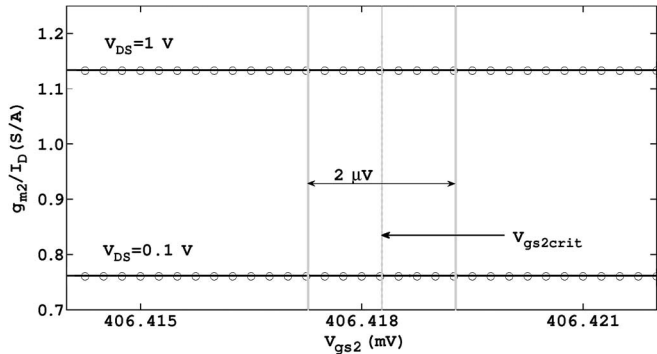


Fig. 3. g_{m2}/I_D around $V_{gs2crit}$ for $V_{gs1} = 1$ V. (Circles) COMSOL data. (Solid lines) Solution by our algorithm. The device parameters are $t_{ox1} = 1$ nm, $t_{ox2} = 2$ nm, and $t_{si} = 10$ nm.

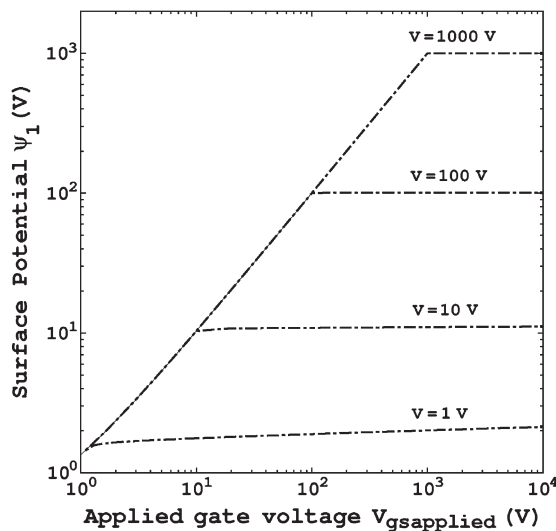


Fig. 4. Surface potential for extreme bias conditions. The device parameters are $t_{ox1} = 1$ nm, $t_{ox2} = 2$ nm, and $t_{si} = 10$ nm. Here, we used the tied gate configuration with $\Delta\phi_1 = 0.56$ and $\Delta\phi_2 = -0.56$.

COMSOL data for the calculation of the surface potential and its derivative for both cases where V_{gs1} is greater and less than V_{gs2} . The analytical expressions for the derivatives are not shown due to space constraints. In Fig. 3, we have shown how the proposed algorithm handles the discontinuity at the GZP. In this figure, we have plotted g_{m2}/I_D , where g_{m2} is the second gate transconductance and I_D is the drain current, against V_{gs2} , while the source end is changing from hyperbolic to trigonometric mode (by varying V_{gs2} around $V_{gs2crit}$ for a step size of 1 nV). Both the characteristics appear to be continuous and match very well with the COMSOL data. It should be noted that, in regime $|V_{gs2} - V_{gs2crit}| < 10^{-6}$, we use the explicit formulation, but beyond this limit, we solve the IVEs numerically. In Fig. 4, we examine the robustness of the proposed algorithm (and the ψ_{gzp} calculation) against extremely high bias voltages, which might appear during circuit simulation. As the overflow and the underflow of math functions under extreme biases are properly covered in the algorithm, it gives an accurate result for any bias conditions.

Due to the presence of several independent variables in the IVEs, it is very difficult to analyze the computation efficiency

of the proposed algorithm. We use the following statistical technique in order to have a fair estimate of the efficiency. For two different devices dev1 and dev2 (having $t_{ox1} = 2$ nm, $t_{ox2} = 3$ nm, and $t_{si} = 30$ nm, and $t_{ox1} = 1$ nm, $t_{ox2} = 1$ nm, and $t_{si} = 10$ nm, respectively), the efficiency of the algorithm is demonstrated in terms of the required number of iterations and computation time by executing it for 1 million random bias points where V_{gs1} and V_{gs2} are varying between 0 and 3 V for a channel voltage of 0 V.

Fig. 5 shows the histogram of the iterations needed (excluding the ψ_{1limit} calculation) to compute ψ_1 for dev1 and dev2, respectively. Bars in black represent samples in the hyperbolic mode, and bars in gray represent that in the trigonometric mode. It can be noticed that convergence is always achieved within ten iterations. It also shows that the probability of using the Ridders algorithm in the hyperbolic mode is very small and the bisection method has never been used. The explicit solution also gets used (although the probability is very small) both in the trigonometric and hyperbolic modes, as indicated by the presence of samples with zero iteration.

Fig. 6 shows the histogram of the total computation time (including the ψ_{1limit} calculation) taken by the samples for nonzero iterations. The histogram is generated by binning the total samples into bins of 0.1-ms width based on the magnitude of their total computation time. Hence, for example, a sample with a 0.32-ms computational time falls into the 0.4-ms bin, and a sample with a 1.15-ms computation time falls into the 1.2-ms bin. It is shown that, in both the devices, the peak in trigonometric samples lags behind the peak in hyperbolic samples by about 9%–15%. Fig. 7 shows the histogram of the percentage of the total computation time taken by the ψ_{1limit} calculation for samples in the trigonometric mode for dev1 and dev2, respectively. On an average, it is shown that the ψ_{1limit} computation, i.e., the overhead computation needed in the trigonometric mode, takes about 10% of the total computation time in both the devices. From Fig. 5, it is shown that the trigonometric and hyperbolic modes peak at the same iteration number. From these observations, it could be concluded that the computation of the trigonometric IVE is slower than that of the hyperbolic IVE because of the iterative ψ_{1limit} calculation in the trigonometric mode.

Finally, in Fig. 8, we show the histogram of the ratio of computational times for the ψ_{gzp1} calculation using the suggested approach to that of the W -function-based approach (as available in the GSL). The suggested approach is found to be much faster than the standard W -function-based approach as only 5% of samples have this ratio more than one.

We have not shown the effect of nonzero V in the above simulation due to the fact that a nonzero (positive) V only shifts the samples from the trigonometric mode to the hyperbolic and explicit modes (which is understandable from the concept of the GZP [5]). For example, when V changes from 0 to 1 V, the percentage of trigonometric samples decrease from about 75% to 50% on an average.

The proposed algorithm is implemented in a commercial circuit simulator [10] through its Verilog-A interface. Fig. 9 depicts the characteristics of an IDG complementary MOS AND gate (NAND gate followed by an inverter) successfully

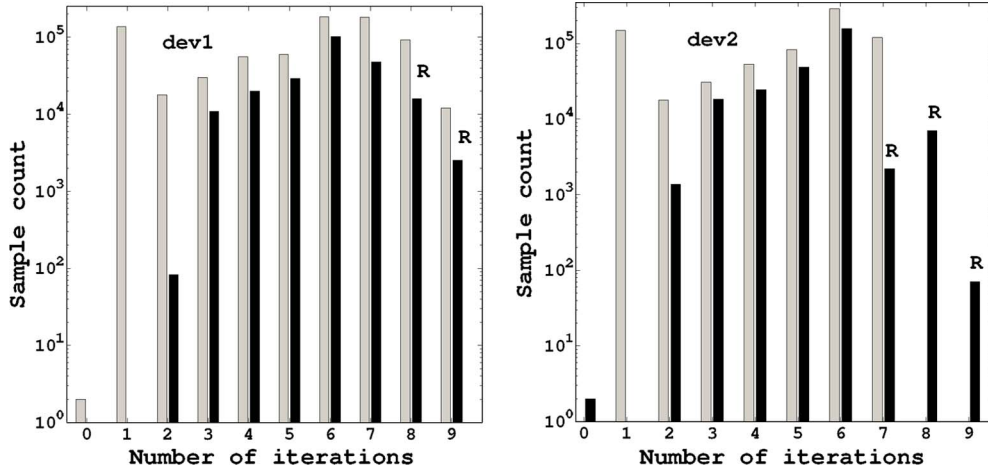


Fig. 5. Histogram of the iterations needed to compute ψ_1 for 1 million samples. Samples in (black bars) hyperbolic mode and (gray bars) trigonometric mode. The Ridder algorithm in the hyperbolic mode is used for samples in the bar represented by “R.” For dev1, 771 011 samples are in the trigonometric mode, whereas for dev2, 739 998 samples are in the trigonometric mode.

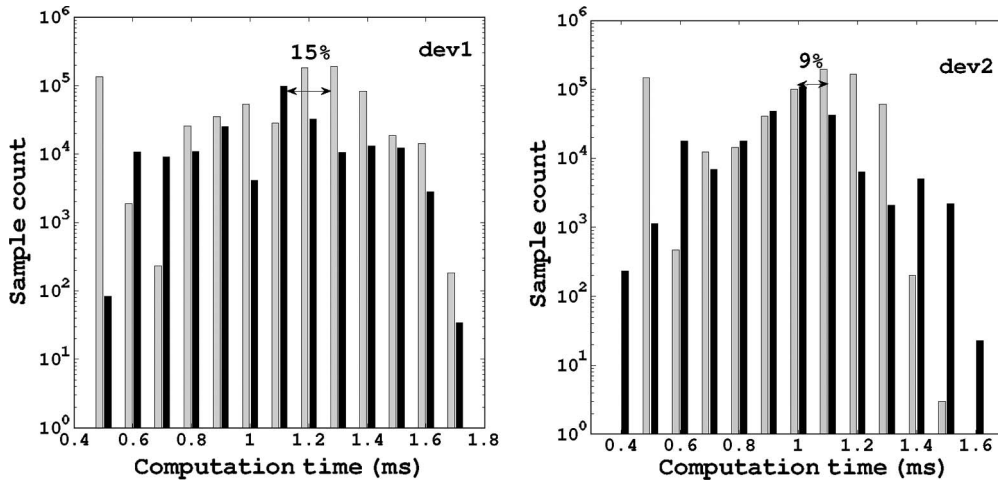


Fig. 6. Histogram of the total computation time for the samples with nonzero iterations. Samples in (black bars) hyperbolic mode and (gray bars) trigonometric mode.

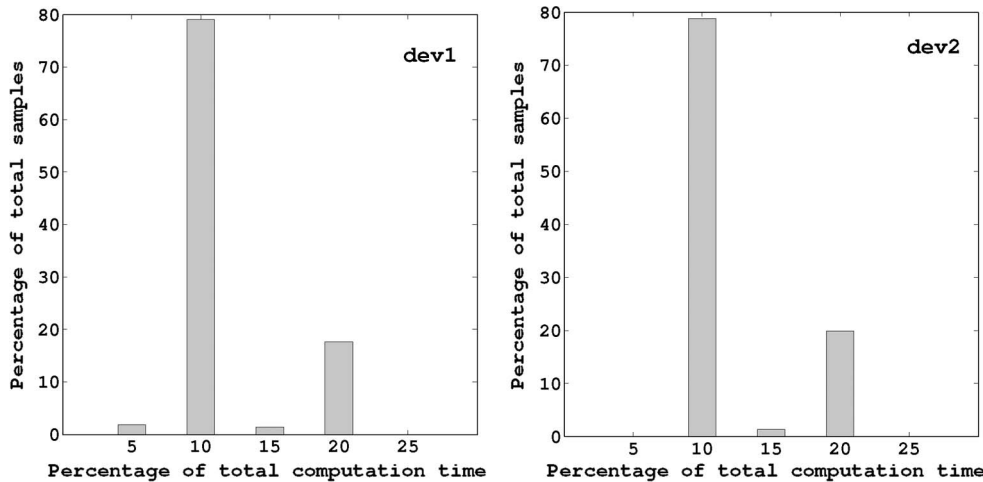


Fig. 7. Histogram of the percentage of the total computation time taken by the $\psi_{1\text{limit}}$ calculation for samples in the trigonometric mode.

simulated using the circuit simulator and verified with the mixed-mode simulation of a technology computer-aided design (TCAD) simulator [11].

In a very recent work [19], effort has been also put to implement those IVEs [5] in a Verilog-A-based circuit simulator with some mathematical conditioning. As the detailed algorithm

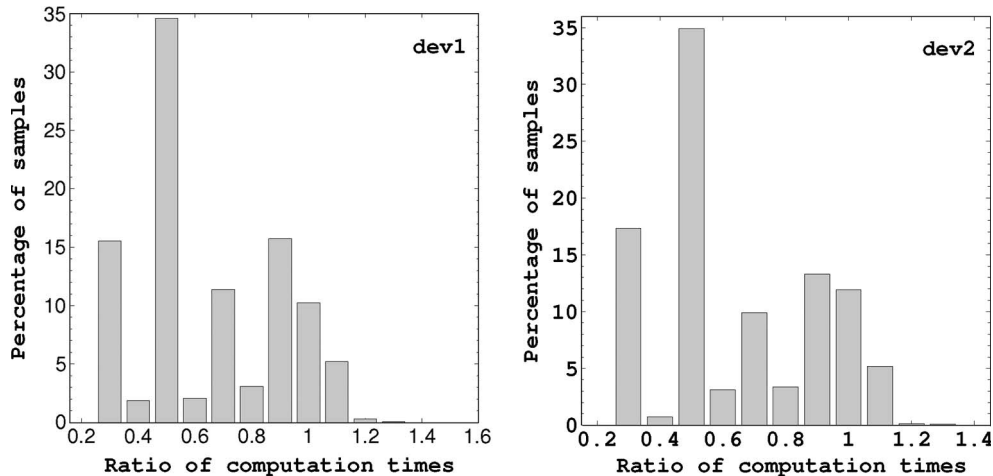


Fig. 8. Histogram depicting the ratio of computational times between the proposed approach to the Lambert-function-based approach for ψ_{gzp1} using a million random bias points using a bin width of 0.1 for binning the ratios.

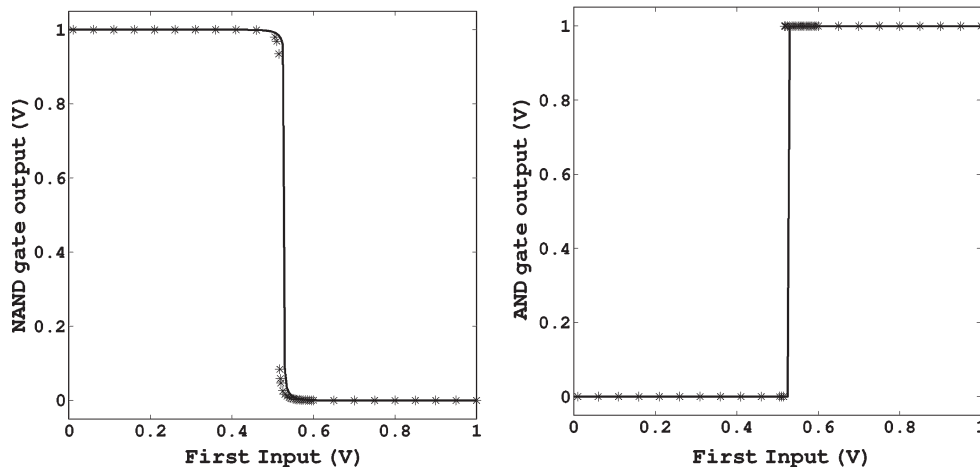


Fig. 9. Simulated characteristics of NAND and AND gates using (line) the circuit simulator and (symbol) the mixed-mode TCAD simulator, keeping the second input at $V_{DD} = 1$ V. Here, we use the same W/L ratio (W is the width, and L is the length of the transistor) for both p- and n-FETs. Yet, the logic transition at $V_{DD}/2$ is achieved by applying suitable second gate voltages (0.8 and 0 V for all p- and n-FETs, respectively). Device parameters used are $t_{ox1} = 1$ nm, $t_{ox2} = 2$ nm, and $t_{si} = 10$ nm.

(initial guess, exit condition, etc.) is not presented, we are not able to compare the proposed algorithm with their work.

IV. CONCLUSION

We have proposed a robust yet efficient root finding algorithm for the IVEs of an IDG MOS transistor without any compromise in accuracy. The proposed algorithm uses a unique approach of root finding by combining the Ridder's algorithm with the NR method in order to provide assured convergence in the presence of discontinuity and singularity in the IVEs. Physics-based optimized input guess, minimized solution space, and regional explicit solution have been used to make the computation faster. The algorithm has been successfully implemented in a commercial circuit simulator and verified against numerical simulations.

ACKNOWLEDGMENT

The authors would like to thank Dr. I. Petic, Chief Executive Officer, Silvaco International, for providing us free access

to the SmartSpice circuit simulator and exclusive support for technology computer-aided design and Spice related queries.

REFERENCES

- [1] H. Lu and Y. Taur, "An analytic potential model for symmetric and asymmetric DG MOSFETs," *IEEE Trans. Electron Devices*, vol. 53, no. 5, pp. 1161–1168, May 2006.
- [2] G. Dessai and G. Gilenblat, "Solution space for the independent-gate asymmetric DGFET," *Solid State Electron.*, vol. 54, no. 4, pp. 382–384, Apr. 2010.
- [3] F. Liu, J. He, Y. Fu, J. Hu, W. Bian, Y. Song, X. Zhang, and M. Chan, "Generic carrier-based core model for undoped four-terminal double-gate MOSFETs valid for symmetric, asymmetric, and independent-gate-operation modes," *IEEE Trans. Electron Devices*, vol. 55, no. 3, pp. 816–826, Mar. 2008.
- [4] A. Ortiz-Conde, F. J. Garcia-Sanchez, J. Muci, S. Malobabic, and J. J. Liou, "A review of core compact models for undoped double gate SOI MOSFETs," *IEEE Trans. Electron Devices*, vol. 54, no. 1, pp. 131–140, Jan. 2007.
- [5] A. Sahoo, P. K. Thakur, and S. Mahapatra, "A computationally efficient generalized Poisson solution for independent double gate transistors," *IEEE Trans. Electron Devices*, vol. 57, no. 3, pp. 632–636, Mar. 2010.
- [6] *MATLAB Version 7.9.0.529 (R2009b)*, 2009.
- [7] T. L. Chen and G. Gilenblat, "Analytical approximation for the MOSFET surface potential," *Solid State Electron.*, vol. 45, no. 2, pp. 335–339, Feb. 2001.

- [8] B. Yu, H. Lu, M. Liu, and Y. Taur, "Explicit continuous models for double-gate and surrounding-gate MOSFETs," *IEEE Trans. Electron Devices*, vol. 54, no. 10, pp. 2715–2722, Oct. 2007.
- [9] C. J. F. Ridders, "Three-point iterations derived from exponential curve fitting," *IEEE Trans. Circuits Syst.*, vol. CAS-26, no. 8, pp. 669–670, Aug. 1979.
- [10] *Smartspice, Analog Circuit Simulator*, ver. 3.6.12.R, Silvaco Int., Santa Clara, CA, 2010. [Online]. Available: www.silvaco.com
- [11] *ATLAS Device Simulation Framework*, ver. 5.17.18.c, Silvaco Int., Santa Clara, CA, 2010. [Online]. Available: www.silvaco.com
- [12] "COMSOL Multiphysics 4.0," *Multiphysics Modeling and Engineering Simulation Software*, 2010. [Online]. Available: <http://www.comsol.com/>
- [13] G. R. Wood, "The bisection method in higher dimensions," *Math. Program.*, vol. 55, no. 3, pp. 319–337, Jun. 1992.
- [14] A. Ortiz-Conde and F. J. Garcia-Sanchez, "Generic complex-variable potential equation for the undoped asymmetric independent double-gate MOSFET," *Solid State Electron.*, vol. 57, no. 1, pp. 43–51, Mar. 2010.
- [15] T. C. Banwell, "Bipolar transistor circuit analysis using the Lambert W-function," *IEEE Trans. Circuits Syst. I, Fundam. Theory Appl.*, vol. 47, no. 11, pp. 1621–1633, Nov. 2000.
- [16] R. Rios, S. Mudanai, W. K. Shih, and P. Packan, "An efficient surface potential solution algorithm for compact MOSFET models," in *IEDM Tech. Dig.*, Dec. 13–15, 2004, pp. 755–758.
- [17] *Users Manual of GNU Scientific Library*, Free Softw. Found., Inc., Boston, MA, 2009.
- [18] W. H. Press, S. A. Teukolsky, W. T. Vetterling, and B. P. Flannery, *Numerical Recipes in C: The Art of Scientific Computing*, 2nd ed. Cambridge, U.K.: Cambridge Univ. Press, 1992, pp. 358–359.
- [19] G. Dessai, W. Wu, B. Bakkaloglu, C. C. McAndrew, and G. Gildenblat, "Compact model and circuit simulations for asymmetric, independent gate FinFETs," *J. Comput. Electron.*, vol. 9, no. 3/4, pp. 103–107, Dec. 2010.



Santanu Mahapatra (M'08–SM'10) received the B.E. degree in electronics and telecommunications from Jadavpur University, Kolkata, India, in 1999, the M.Tech. degree in electrical engineering, with specialization in microelectronics, from the Indian Institute of Technology, Kanpur, India, in 2001, and the Ph.D. degree in electrical engineering from the Swiss Federal Institute of Technology-Lausanne (EPFL), Lausanne, Switzerland, in 2005. His Ph.D. work was focused on the compact modeling of single-electron transistors and their hybridization

with complementary metal–oxide–semiconductor (CMOS).

In August 2005, he was an Assistant Professor with the Center for Electronics Design and Technology (CEDT), Indian Institute of Science, Bangalore, India, where he has been an Associate Professor since September 2010, promoted on an out-of-the-term basis. In 2006, he founded the Nano Scale Device Research Laboratory, CEDT, where his team is currently engaged in the research on the compact modeling and simulation of emerging nanotechnologies and advanced CMOS devices. He has supervised many students for their M.S. thesis and Ph.D. dissertation. He is the author or a coauthor of several papers published in international journals and refereed conference proceedings. He is also the author of the book *Hybrid CMOS Single Electron Transistor Device and Circuit Design* (Artech House, 2006). His current research interests include device reliability, multigate transistors, tunnel field-effect transistors, single-electron transistors, carbon nanoelectronics, and CMOS nanohybridization.

Prof. Mahapatra was the recipient of the Best Paper Award at the International Semiconductor Conference, Romania, in 2003, an IBM Faculty Award in 2007, the Microsoft India Research Outstanding Faculty Award in 2007, and the Associateship of the Indian Academy of Science in 2009.



Srivatsava Jandhyala received the M.S. degree in physics and the M.Sc. (Engg) in electronics in 2001 and 2004, respectively, from the Indian Institute of Science, Bangalore, India, where he is currently working toward the Ph.D. degree in the Nano Scale Device Research Laboratory, Center for Electronics Design and Technology.

He worked on application-specified integrated-circuit physical design for more than seven years across companies such as Broadcom, Freescale, and Intel Technologies India Pvt. Ltd., Bangalore, India.

He is focused on issues related to the compact modeling of double-gate metal–oxide–semiconductor field-effect transistors.